

# An Unsupervised Normalizing Flow-Based Neyman-Pearson Detector for Covert Communications in the Presence of Disco Reconfigurable Intelligent Surfaces

Luyao Sun, Sitian Li, Huan Huang, *Member, IEEE*, Hongliang Zhang, *Member, IEEE*, Weidong Mei, *Member, IEEE*, Dongdong Zou, Jun Li, *Member, IEEE*, Gangxiang Shen, *Senior Member, IEEE*, Yi Cai

**Abstract**—Covert communications, also known as low probability of detection (LPD) communications, offer a higher level of privacy protection compared to cryptography and physical-layer security (PLS) by hiding the transmission within ambient environments. Here, we investigate covert communications in the presence of a disco reconfigurable intelligent surface (DRIS) deployed by the warden Willie, which simultaneously reduces his detection error probabilities and degrades the communication performance between Alice and Bob, without relying on either channel state information (CSI) or additional jamming power. However, the introduction of the DRIS renders it intractable for Willie to construct a Neyman-Pearson (NP) detector, since the probability density function (PDF) of the test statistic is analytically intractable under the Alice-Bob transmission hypothesis. Moreover, given the adversarial relationship between Willie and Alice/Bob, it is unrealistic to assume that Willie has access to a labeled training dataset. To address these challenges, we propose an unsupervised masked autoregressive flow (MAF)-based NP detection framework that exploits prior knowledge inherent in covert communications. We further define the false alarm rate (FAR) and the missed detection rate (MDR) as monitoring performance metrics for Willie, and the signal-to-jamming-plus-noise ratio (SJNR) as a communication performance metric for Alice-Bob transmissions. Furthermore, we derive theoretical expressions for SJNR and uncover unique properties of covert communications in the presence of a DRIS. Simulations validate the theory and show that the proposed unsupervised MAF-based NP detector achieves performance comparable to its supervised counterpart.

**Keywords**—Covert communications, reconfigurable intelligent surface, physical layer security, Neyman-Pearson detection, channel aging

## 1 Introduction

Due to the inherent properties of wireless channels, such as broadcast and superposition, wireless communication systems are vulnerable to malicious attacks [1]. This vulnerability is particularly critical in the context of the Internet of Things (IoT), where transmitted signals often carry sensitive personal information, including healthcare records and location information. Maintaining communication confidentiality is also imperative for security-sensitive applications, particularly in government and the military. As a result, considerable research attention has been devoted to developing techniques that enhance transmission security and safeguard user privacy [2]. Covert communications have emerged as a promising strategy [3-5], which aims to conceal the very existence of transmitted signals by embedding them in ambient noise or legitimate traffic, thereby significantly reducing their probability of detection and their susceptibility to adversarial interference. Unlike conventional cryptographic techniques and physical-layer security (PLS) mechanisms, which primarily protect the confidentiality of transmitted content, covert

---

This work was supported by the National Key Research and Development Program of China under Grant No. 2022YFB2903000, and the National Natural Science Foundation of China under Grant Nos. 62250710164, 62275185, and 62371011, and in part by the Natural Science Foundation of Jiangsu Province under Grant No. BK20240768.

L. Sun, S. Li, H. Huang, D. Zou, J. Li, Y. Cai, and G. Shen are with the School of Electronic and Information Engineering, Soochow University, Suzhou, Jiangsu 215006, China (e-mail: lysun02@163.com, 19301560802@163.com, hhuang1799@gmail.com, ddzou@suda.edu.cn, ljun@suda.edu.cn, yicai@ieee.org, shengx@suda.edu.cn).

H. Zhang is with the School of Electronics, Peking University, Beijing 100871, China (e-mail: hongliang.zhang92@gmail.com).

W. Mei is with the National Key Laboratory of Wireless Communications, University of Electronic Science and Technology of China, Chengdu 611731, China (e-mail: wmei@uestc.edu.cn).

communications offer stronger privacy by concealing whether communication occurs at all.

In [6], the authors established the fundamental square-root law of covert communications: at most  $o(\sqrt{n})$  bits can be covertly transmitted over  $n$  additive white Gaussian noise (AWGN) channel uses while ensuring an arbitrarily low probability of detection (LPD) without knowledge of the channel noise power between the transmitter Alice and the warden Willie, where  $o(\sqrt{n})$  represents a non-asymptotically tight upper bound on  $\sqrt{n}$ . Following the work in [6], some works have introduced techniques such as non-orthogonal multiple access (NOMA) and turbo encoding to improve the performance of covert communication systems [7,8]. Existing studies [9-11] have examined the use of jammers or artificial noise to increase observation uncertainty at the warden Willie, thereby making it harder for Willie to reliably detect Alice's activity. Relay-assisted schemes [12-14] can also degrade the separability of Willie's hypothesis test, which raises his detection error probabilities. In addition, the work in [15] proposed that exploiting small-scale-fading-induced power variability to reduce Willie's detection reliability and attain LPD.

Recently, reconfigurable intelligent surfaces (RISs) have emerged as a promising approach to improving the performance and efficiency of wireless communication systems [16-21]. An RIS typically comprises a large number of reflecting elements that can dynamically adjust the amplitude and phase of incident signals through low-cost components such as PIN or varactor diodes [22]. The integration of RIS into wireless networks provides considerable performance gains without incurring significant increases in power consumption or deployment costs [23], [24]. Recently, Moreover, RIS-assisted covert communications have also gained growing research interest [25-29]. Previous studies have explored the use of single or multiple RISs to enhance covertness in diverse systems, including those leveraging NOMA [25], artificial noise [26], finite blocklength coding with adaptive priors [27], and unmanned aerial vehicle (UAV)-based networks [28], [29].

Existing research on covert communications, with or without RISs, generally assumes channel reciprocity in time-division duplex (TDD) systems and treats it as exact or approximately valid. Although widely adopted, this assumption no longer holds when using time-varying disco RIS (DRIS) [30] or RIS architectures with non-reciprocal inter-element connections [31]. The use of a DRIS in covert communications was first proposed in [32], where random and time-varying DRIS acts like a “disco ball” and then generates active channel aging (ACA), which breaks TDD channel reciprocity even within the channel coherence time. A DRIS can be implemented without requiring either channel state information (CSI) or additional jamming power. At the same time, it reduces the probability of detection by Warden Willie and degrades the communication performance between Alice

and Bob [32]. The introduction of DRIS breaks the following two fundamental premises of conventional covert communications: (i) TDD channel reciprocity is intentionally aged even within a channel coherence interval, rendering existing threshold designs based on static statistical models inapplicable; and (ii) the distribution of the test statistic under Alice-Bob transmission (i.e., under hypothesis  $\mathcal{H}_1$ ) no longer admits a closed-form expression [32].

Normalizing flows (NFs) employ bijective transformations with computationally tractable Jacobian determinants, thereby enabling exact likelihood estimation for complex data distributions [33]. Notable architectural variants include autoregressive models such as the masked autoregressive flow (MAF) [34] and the inverse autoregressive flow (IAF) [35], coupling-based models such as RealNVP [33], and multi-scale invertible architectures such as Glow [36]. Therefore, in principle, Warden Willie could leverage NFs to determine the intractable distribution of the test statistic under the  $\mathcal{H}_1$ . This would enable the construction of a Neyman-Pearson (NP) detector that would remain theoretically optimal even in the presence of DRIS-induced ACA. Unfortunately, the training of NFs typically requires labeled datasets, where each sample is explicitly annotated with its corresponding hypothesis, i.e., whether it was obtained under Alice-Bob transmission or under silence (hypothesis  $\mathcal{H}_0$ ). In covert communication scenarios where Alice and Bob operate adversarially against Willie, the assumption of labeled datasets is unrealistic because Willie has no reliable access to ground-truth information about Alice's activity.

In this work, we propose a novel unsupervised MAF-based NP detector, built by Willie, to detect the covert communications in the presence of a DRIS. The main contributions of this paper are summarized as follows.

- We first formulate the covert communication model in the presence of a DRIS, where the DRIS with random and time-varying reflection coefficients acts like a “disco ball” and operates autonomously without any connection or coordination. The introduction of the DRIS not only jams the covert communications between Alice and Bob but also reduces the decision error probabilities, i.e., the false alarm rate (FAR) and missed detection rate (MDR) at the warden Willie, without relying on either Alice-Bob channel knowledge or additional jamming power. To quantify the impact of DRIS on covert communications, we use the FAR and MDR to monitor the detection performance at Willie and the signal-to-jamming-plus-noise ratio (SJNR) to characterize the communication performance at Bob.

- For covert communications in the presence of a DRIS, the probability density function (PDF) of the test statistic at the warden Willie is analytically intractable when Alice and Bob are communicating. As a result, the NP detector con-

structed based on the PDFs under the hypothesis  $\mathcal{H}_1$  (i.e., Alice-Bob transmission) and the hypothesis  $\mathcal{H}_0$  (i.e., Alice is silent) can not be directly obtained. Considering the adversarial nature between the warden Willie and the covert communication parties (Alice and Bob), it is unrealistic to assume that Willie can obtain a labeled training dataset, i.e., one that distinguishes samples collected under  $\mathcal{H}_1$  and  $\mathcal{H}_0$ . To this end, we propose an unsupervised MAF-based NP detection framework. Specifically, we exploit the prior knowledge inherent in covert communications that, under  $\mathcal{H}_0$ , Willie's received signal consists solely of noise, and then design an unsupervised MAF to estimate the PDF of the test statistic under  $\mathcal{H}_1$ .

- As Willie is generally adversarial toward Alice and Bob, being able to jam their communication whenever it occurs offers him a strategic advantage. The DRIS deployed by Willie can also significantly degrade the SJNR at Bob. Based on the derived statistical characteristic of the cascaded DRIS channel, an asymptotic analysis of the SJNR is conducted to demonstrate the impact of the DRIS on covert communications between Alice and Bob. Simulation results validate the theoretical analyses and show that the proposed unsupervised MAF-based NP detector performs comparably to a supervised MAF-based NP detector. Moreover, we present some unique properties of DRIS. For example, increasing the transmit power at Alice can not significantly increase the SJNR at Bob due to the DRIS. Instead, it exacerbates the impact of DRIS-induced ACA on the covert communications, and increases Alice's risk of detection by Willie. In addition, a DRIS with only 1-bit phase quantization is sufficient to improve the detection accuracy at Willie and degrade the communication performance between Alice and Bob.

The rest of this paper is organized as follows. In Section 2, we first present the covert communication model in the presence of a DRIS and build the channel models of all wireless channel. We then derive Willie's decision rule and adopt the false alarm rate (FAR) and missed detection rate (MDR) as his detection metrics; the signal-to-jammer-plus-noise ratio (SJNR) is used to quantify the communication performance. Some useful results on signal detections and random variables are presented. In Section 3, we outline the challenges that the DRIS introduces to Willie's detection. In other words, the PDF of the test standards under  $\mathcal{H}_1$  is analytically intractable. To address this challenge, we propose an unsupervised MAF-based NP detection framework that exploits prior knowledge in covert communications. Furthermore, we derive the statistical characteristic of DRIS-induced ACA and conduct an asymptotic analysis of the SJNR at Bob as quantifying the communication performance between Alice and Bob. In Section 4, the simulation and theoretical results are compared to validate the derived theoretical analyses and verify the feasibility of the proposed unsupervised MAF-based NP detection

framework. Finally, conclusions are given in Section 5.

*Notation:* We use lowercase boldface letters for vectors (e.g.,  $\mathbf{g}$ ) and italic letters for scalars (e.g.,  $N_D$ ). The operators  $(\cdot)^T$  and  $(\cdot)^H$  denote the transpose and the Hermitian transpose, respectively. The symbol  $|\cdot|$  denotes absolute value, and  $\mathbb{E}[\cdot]$  denotes statistical expectation.

## 2 System Description

In Section 2, we first present the covert communication model in the presence of a DRIS and build the channel models of all wireless channel involved in Section 2.1. In Section 2.2, the decision rule adopted by the warden Willie is first defined. Then, the FAR and MDR are given as monitoring performance metrics for Willie, while the SJNR is defined as a communication performance metric. In Section 2.3, some useful results on signal detections and random variables are presented.

### 2.1 Covert Communications in the Presence of a DRIS

Fig. 1 schematically illustrates a covert communication system, in which Willie simultaneously attempts to detect and jam the transmission between Alice and Bob via a DRIS, simultaneously. In covert communications, Alice tries to covertly transmit a message to Bob without being detected by the warden Willie, while also maintaining the highest possible communication quality [5,6]. In contrast, Willie aims to detect the covert communications between Alice and Bob as accurate as possible. In this work, we consider a robust covert communication scenario where the warden has no knowledge of the Alice-to-Bob channel, such as their locations. Namely, Willie attempts to detect potential covert communications without any coordination with Alice or Bob. Furthermore, we assume that it is not feasible to obtain a labeled dataset for training a detection model for Willie. These assumptions enhance the robustness of our proposed scheme, making it ideal for practical covert communication scenarios.

The warden Willie employs an  $N_D$ -element DRIS with random and time-varying coefficient configurations to improve the detection accuracy of covert communications. Notably, even in cases where the warden fails to detect the covert communications, the presence of DRIS can still impose significant ACA on the communications between Alice and Bob. The resulting DRIS-induced ACA impact is analyzed in subsequent sections. In the DRIS, its coefficients are assumed to be adjusted by the programmable PIN [22], whose ON/OFF behavior only allows for the implementation of a discrete DRIS coefficient adjustment. More specifically, we assume that the DRIS has  $b$ -bit quantization phase shifts and amplitude values. The phase shift

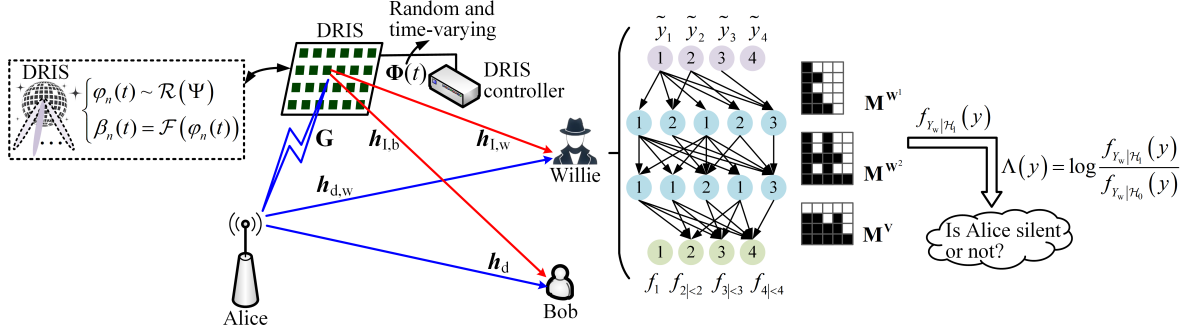


**Figure 1** Covert communications in the presence of a disco reconfigurable intelligent surface (DRIS), where the DRIS with time-varying and random reflection coefficients is generated by a DRIS controller and the warden Willie employs normalizing flows to assist in his detection.

and amplitude sets are denoted as  $\Omega = \{\phi_1, \phi_2, \dots, \phi_{2^b}\}$  and  $\Lambda = \{\alpha_1, \alpha_2, \dots, \alpha_{2^b}\}$ , respectively. Consequently, the random and time-varying DRIS coefficients can be expressed as  $\varphi(t) = [\beta_1(t)e^{\varphi_1(t)}, \beta_2(t)e^{\varphi_2(t)}, \dots, \beta_{N_D}(t)e^{\varphi_{N_D}(t)}]$ , where the time-varying of the  $r$ -th DRIS element follows a stochastic distribution  $\mathcal{R}$ , i.e.,  $\varphi_r(t) \sim \mathcal{R}(\Omega)$ . In practice, the amplitudes  $\beta_r(t)$ , ( $r = 1, 2, \dots, N_D$ ) is typically dependent on the corresponding phase shift and can be modeled as  $\beta_r(t) = \mathcal{F}(\varphi_r(t))$ , where  $\mathcal{F}$  is a deterministic mapping determined by hardware characteristics.

In covert communications, Willie attempts to determine from his observations which of the following two hypotheses holds: Alice is transmitting ( $\mathcal{H}_1$ ), or Alice is silent ( $\mathcal{H}_0$ ). Referring to the covert communication model in [25], the  $m$ -th received signal at the warden Willie can be expressed as

$$y_w(m) = \begin{cases} \underbrace{h_d^w s(m)}_{\text{Direct link}} + \underbrace{h_D^w(m) s(m)}_{\text{DRIS-Based link}} + n_w(m) & \mathcal{H}_1, \\ n_w(m) & \mathcal{H}_0, \end{cases} \quad (1)$$

where  $s(m)$  denotes the  $m$ -th covert symbol transmitted by Alice within a channel coherence interval, and  $n_w(m)$  represents the additive white Gaussian noise (AWGN) with zero mean and variance  $\delta_w^2$ , i.e.,  $n_w(m) \sim \mathcal{CN}(0, \delta_w^2)$ . Similar to [3-5], the covert symbols transmitted by Alice are modeled as independent and identically distributed (i.i.d.) complex Gaussian random variables zero mean and variance  $P_0$ , i.e.,  $s(m) \sim \mathcal{CN}(0, P_0)$ , where  $P_0$  denotes the transmit power of the covert symbols.

In (1),  $h_d^w = \hat{h}_d^w / \mathcal{L}^{\frac{v_w}{2}}$  denotes the direct channel between Alice and Willie, where  $\hat{h}_d^w$  represents the small-scale fading coefficient and  $\mathcal{L}^{\frac{v_w}{2}}$  denotes the large-scale fading coefficient, respectively. Moreover,  $h_D^w(t)$  denotes the cascaded DRIS-based channel between Alice and Willie. Specifically,

$h_D^w(t)$  can be further expressed as

$$h_D^w(t) = g \text{diag}(\varphi(t)) h_I^w \quad (2)$$

$$= \frac{\hat{g}}{\mathcal{L}^{\frac{v_g}{2}}} \text{diag}(\varphi(t)) \frac{\hat{h}_I^w}{\mathcal{L}^{\frac{v_I^w}{2}}}, \quad (3)$$

where  $\mathcal{L}^{\frac{v_g}{2}}$  and  $\mathcal{L}^{\frac{v_I^w}{2}}$  represent the large-scale fading coefficients of the Alice-DRIS channel and the DRIS-Willie channel, respectively. Furthermore, the elements in  $\hat{h}_I^w$  are assumed to be i.i.d. following a complex Gaussian distribution, i.e.,  $\hat{h}_I^w \sim \mathcal{CN}(\mathbf{0}, \mathbf{I}_{N_D})$ , where  $\mathbf{I}_{N_D}$  is the  $N_D \times N_D$  identity matrix.

In this work, we assume that the DRIS is deployed close to Alice to maximize its impact as much as possible. Furthermore, the DRIS is typically equipped with a large number of reflective elements to compensate for the severe multiplicative large-scale fading of the cascaded DRIS-based channel [30,37,38]. Consequently,  $\hat{h}_I^w$  is built based on the near-field model [39,40], i.e.,

$$\hat{g} = \sqrt{\frac{\kappa_g}{1 + \kappa_g}} \hat{g}^{\text{LOS}} + \sqrt{\frac{1}{1 + \kappa_g}} \hat{g}^{\text{NLOS}}, \quad (4)$$

where  $\kappa_g$  denotes the Rician factor for Alice-DRIS channel. On the one hand, the elements in the non-line-of-sight (NLOS) component  $\hat{g}^{\text{NLOS}}$  are assumed to be i.i.d. complex Gaussian random variables, i.e.,  $\hat{g}^{\text{NLOS}} \sim \mathcal{CN}(\mathbf{0}, \mathbf{I}_{N_D})$ . On the other hand, the elements in the line-of-sight (LOS) component  $\hat{g}^{\text{LOS}}$  can be given by

$$[\hat{g}^{\text{NLOS}}]_r = e^{-j \frac{2\pi}{\lambda} (d_r - d_0)}, \quad (5)$$

where  $r = 1, \dots, N_D$ ,  $\lambda$  is the wavelength of the transmitted covert signals,  $d_r$  and  $d_0$  denote the distance between Alice's antenna and the  $r$ -th DRIS element, and the distance between this antenna and the centre of the DRIS, respectively.

In this covert communication scenario, we assume that Bob is aware of whether Alice is transmitting or not. Accordingly,

if Alice remains silent, Bob does not attempt to receive any signal. More specifically, when  $M$  covert symbols are transmitted by Alice, the received signal at Bob can be expressed as

$$y_b(m) = \underbrace{h_d^b s(m)}_{\text{Covert symbol}} + \underbrace{h_D^b(m) s(m)}_{\text{DRIS jamming}} + \underbrace{n_b(m)}_{\text{Noise}} \quad (6)$$

$$= \frac{\widehat{h}_d^b s(m)}{\mathcal{L}^{\frac{v_d^b}{2}}} + \frac{\widehat{g} \text{diag}(\varphi(m)) \widehat{h}_I^b s(m)}{\mathcal{L}^{\frac{v_g}{2}} \mathcal{L}^{\frac{v_d^b}{2}}} + n_b(m), \quad (7)$$

where  $m = 1, 2, \dots, M$ ,  $\mathcal{L}^{\frac{v_d^b}{2}}$  and  $\mathcal{L}^{\frac{v_g}{2}}$  respectively represent the large-scale fading coefficients of the Alice-Bob channel and the DRIS-Bob channel, and  $n_b(m)$  is the AWGN with zero mean and variance  $\delta_b^2$ . More specifically,  $\widehat{h}_d^b$  and  $\widehat{h}_I^b$  in (7) are assumed to follow complex Gaussian distributions, given by  $\widehat{h}_d^b \sim \text{CN}(0, 1)$  and  $\widehat{h}_I^b \sim \text{CN}(\mathbf{0}, \mathbf{I}_{N_D})$ , respectively.

## 2.2 Detection and Communication Performance Metrics

To evaluate Willie's detection performance in covert communications in the presence of the DRIS, we define the detection error probabilities [4,13,14,25,28], i.e., the MDR and the FAR as the detection performance metrics. To assess the quality of covert communication between Alice and Bob, the SJNR [38] is used as the communication performance metric.

Mathematically, based on the received symbols at Willie given in (1), the decision rule adopted by the warden Willie can be expressed by

$$Y_w = \sum_{n=1}^N |y_w(n)|^2 \begin{cases} \mathcal{H}_1 \\ \mathcal{H}_0 \end{cases} \quad (8)$$

where  $N$  denotes the total number of detection samples satisfying  $N \leq M$ , and  $\eta_o$  represents the predefined detection threshold. Consequently, the MDR denoted by  $p_M$  is the probability that Alice and Bob are transmitting while the warden incorrectly assumes that they are silent, i.e.,

$$p_M = \mathbb{P} \left( \sum_{n=1}^N |y_w(n)|^2 < \eta_o \middle| \mathcal{H}_1 \right). \quad (9)$$

Meanwhile, the FAR denoted by  $p_F$  is the probability that Alice and Bob are silent while the warden incorrectly assumes that they are transmitting, i.e.,

$$p_F = \mathbb{P} \left( \sum_{n=1}^N |y_w(n)|^2 \geq \eta_o \middle| \mathcal{H}_0 \right). \quad (10)$$

Moreover, the ergodic SJNR at Bob can be defined based

on (7) as follows:

$$\gamma_b = \frac{\mathbb{E} \left[ \left| \frac{\widehat{h}_d^b s(m)}{\mathcal{L}^{\frac{v_d^b}{2}}} \right|^2 \right]}{\mathbb{E} \left[ \left| \frac{\widehat{g} \text{diag}(\varphi(m)) \widehat{h}_I^b s(m)}{\mathcal{L}^{\frac{v_g}{2}} \mathcal{L}^{\frac{v_d^b}{2}}} \right|^2 \right] + \delta_b^2}. \quad (11)$$

From (9) to (11), it can be observed that the introduction of the DRIS not only influences the optimal detection threshold but also degrades the ergodic SJNR at Bob. In Section 3, we present an unsupervised MAF-based Neyman-Pearson detector to determine the optimal detection threshold and quantitatively evaluate the impact of the DRIS on the communication performance.

## 2.3 Preliminary: Review of Some Related Results

**Lemma 1** (Neyman-Pearson Lemma) Let  $X$  be a random variable whose distribution under the null hypothesis  $\mathcal{H}_0$  is  $f_0(x)$ , and under the alternative hypothesis  $\mathcal{H}_1$  is  $f_1(x)$ , where both  $\mathcal{H}_0$  and  $\mathcal{H}_1$  are simple hypotheses. Then, for any significance level  $\alpha \in [0, 1]$ , the most powerful test among all tests of level  $\alpha$  is given by the likelihood ratio (LLR) test:

$$\phi(x) = \begin{cases} 1, & \text{if } \Lambda(x) > \eta \\ \gamma, & \text{if } \Lambda(x) = \eta \\ 0, & \text{if } \Lambda(x) < \eta \end{cases} \quad (12)$$

where  $\Lambda(x) = \frac{f_1(x)}{f_0(x)}$  is the LLR,  $\eta$  is a threshold chosen to satisfy the constraint  $\mathbb{E}[\phi(X)] = \alpha$ , and  $\gamma \in [0, 1]$  is a randomization probability to ensure the test has exact level  $\alpha$  when needed.

**Theorem 1** (Lindeberg-Lévy Central Limit Theorem) Suppose  $\mathbf{x} \triangleq [x_1, x_2, \dots, x_n]$  is a vector of i.i.d. random variables with mean  $\mathbb{E}[x_1] = \mathbb{E}[x_2] = \dots = \mathbb{E}[x_n] = \mu < \infty$  and variance  $\text{Var}[x_1] = \text{Var}[x_2] = \dots = \text{Var}[x_n] = v^2 < \infty$ . According to the Lindeberg-Lévy central limit theorem, the random variable  $\sqrt{n}(\bar{X} - \mu)$  converges in distribution to  $\text{CN}(0, v^2)$  as  $n \rightarrow \infty$ , i.e.,

$$\sqrt{n}(\bar{X} - \mu) = \frac{\sum_{i=1}^n x_i}{\sqrt{n}} - \sqrt{n}\mu \xrightarrow{d} \text{CN}(0, v^2), \text{ as } n \rightarrow \infty. \quad (13)$$

## 3 Simultaneously Exposing and Jamming Covert Communications

In Section 3, we first state the challenges imposed by the DRIS into the Willie detection, where the introduction of the

DRIS makes it analytically intractable to give the PDF of received samples at the warden Willie under  $\mathcal{H}_1$  in Section 3.1. In Section 3.2, we proposed an unsupervised MAF-based NP detection framework to estimate the PDF of the test statistic under  $\mathcal{H}_1$  by exploiting the prior knowledge inherent in covert communications. In Section 3.3, we first derive the statistical characteristic of DRIS-induced ACA and then conduct an asymptotic analysis of the SJNR at Bob as quantifying the communication performance between Alice and Bob.

### 3.1 Impact of DRIS on Willie's detection

Recalling the detection at Willie expressed by (8), it is a typical binary hypothesis testing. When Alice is silent, i.e.,  $\mathcal{H}_0$ , the observation  $Y_w$  is specifically reduced to

$$Y_w = \sum_{n=1}^N |n_w(n)|^2. \quad (14)$$

Conditioned on the fact that the random variables  $n_w(n)$  are the AWGN, the observation  $Y_w$  follows a Gamma distribution with a shape parameter  $N$  and a scale parameter  $\delta_w^2$ , i.e.,  $Y_w \sim \text{Gamma}(N, \delta_w^2)$ . Furthermore, the PDF of  $Y_w$  under  $\mathcal{H}_0$  is given by

$$f_{Y_w|\mathcal{H}_0}(y) = \frac{1}{\Gamma(N)(\delta_w^2)^N} y^{N-1} e^{-\frac{y}{\delta_w^2}}, y \geq 0, \quad (15)$$

where  $\Gamma(\cdot)$  represents the Gamma function. Since  $N$  in (15) is a positive integer,  $\Gamma(N)$  can be reduced to  $\Gamma(N) = (N-1)!$ , where  $(N-1)!$  denotes the factorial of  $(N-1)$ .

If the PDF of the observation  $Y_w$  under the alternative hypothesis  $\mathcal{H}_1$  can be obtained, based on the Neyman-Pearson Lemma, the optimal decision threshold  $\eta_o$  can be obtained. Before giving the PDF of the observation  $Y_w$  under  $\mathcal{H}_1$ , we derive the asymptotic distribution of the cascade DRIS-based channel  $h_D^w(t)$  in (2), which is given in the following Proposition 1.

**Proposition 1** The random and time-varying DRIS-based term  $h_D^w(t)$  converges in distribution to a complex Gaussian distribution as  $N_D \rightarrow \infty$ , i.e.,

$$h_D^w(t) = \frac{\widehat{g}\text{diag}(\varphi(t))\widehat{h}_I^w}{\mathcal{L}^{\frac{v_g}{2}}\mathcal{L}^{\frac{v_I^w}{2}}} \xrightarrow{d} \mathcal{CN}\left(0, \frac{N_D\bar{\alpha}}{\mathcal{L}^{v_g}\mathcal{L}^{v_I^w}}\right). \quad (16)$$

In (16),  $\bar{\alpha} = \sum_{i=1}^{2^b} p_i \alpha_i^2$ , where  $p_i$  is the probability of the  $r$ -th DRIS phase shift  $\varphi_r(t)$  ( $r = 1, 2, \dots, N_D$ ) taking the  $i$ -th value of  $\Omega$ , i.e.,  $\mathbb{P}(\varphi_r(t) = \phi_i), \forall n$ .

**Proof** See Appendix 5.1.

Unfortunately, according to Proposition 1, the deployment of the DRIS prevents Willie from deriving an explicit expression for the PDF of  $Y_w$  under  $\mathcal{H}_1$ , i.e.,  $f_{Y_w|\mathcal{H}_1}(y)$ . It is worth noting that the DRIS jamming term in (1), i.e.,  $Z_w =$

$h_D^w(m)s(m)$ , can be viewed as a new random variable resulting from the product of two independent complex Gaussian random variables. However, the product of two independent complex Gaussian variables is not itself Gaussian [41]. Given two independent complex random variables  $X$  and  $Y$  with PDFs  $f_X(x)$  and  $f_Y(y)$ , respectively, the PDF of  $Z = XY$  can be computed as

$$f_Z(z) = \int_{\mathbb{C}} f_X(x) f_Y\left(\frac{z}{x}\right) \frac{1}{|x|^2} d^2x. \quad (17)$$

Consequently, the PDF of  $Z_w$  can be calculated as

$$f_{Z_w}(z) = \frac{1}{\pi^2 P_0 \frac{N_D \bar{\alpha}}{\mathcal{L}^{v_g} \mathcal{L}^{v_I^w}}} \times \int_{\mathbb{C}} \exp\left\{-\frac{|x|^2}{\frac{N_D \bar{\alpha}}{\mathcal{L}^{v_g} \mathcal{L}^{v_I^w}}}\right\} \exp\left\{-\frac{|z|^2}{P_0}\right\} \frac{1}{|x|^2} d^2x. \quad (18)$$

Moreover, in (1) under  $\mathcal{H}_1$ , the sum of the received covert symbol and the noise can be treated as a new complex Gaussian random variable, i.e.,  $N_w = h_d^w s(m) + n_w(m) \sim \mathcal{CN}\left(0, |h_d^w|^2 P_0 + \delta_w^2\right)$ . Note that, given two independent complex random variables  $X$  and  $Y$  with PDFs  $f_X(x)$  and  $f_Y(y)$ , respectively, the PDF of  $Z = X + Y$  can be calculated as

$$f_Z(z) = \int_{\mathbb{C}} f_X(x) f_Y(z-x) d^2x. \quad (19)$$

Theoretically, the  $m$ -th received signal at Willie under  $\mathcal{H}_1$ , i.e.,  $y_w(m) = Z_w + N_w$ , can be regarded as a random variable whose PDF can be calculated using (19). Unfortunately, based on (18) and (19), it is difficult to derive an explicit expression for the PDF of  $y_w(m)$  due to the mathematical intractability of the product and sum of complex random variables involved. As a result, it is also difficult to derive a closed-form expression for the PDF of  $Y_w$  under  $\mathcal{H}_1$ . Therefore, in the covert communication system in the presence of a DRIS, the optimal decision threshold  $\eta_o$  can not be directly obtained based on the Neyman-Pearson lemma.

### 3.2 Unsupervised MAF-Based Density Estimation for Optimal Detection at Willie

Note that the chain rule of probability makes sure that any PDF  $f(x)$  can be decomposed into a product of conditional PDFs as

$$f_{Y_w|\mathcal{H}_1}(y) = f(y_1) \prod_{t=2}^T f(y_t|y_1, \dots, y_{t-1}). \quad (20)$$

In this work, we treat each  $y$  (i.e., an observation  $Y_w$  under  $\mathcal{H}_1$ ) as a scalar statistic and therefore train a one-dimensional flow ( $d=1$ ) to approximate the marginal density  $f_{Y_w|\mathcal{H}_1}(y)$ . Directly parameterising every conditional PDF is impractical,

MAF embeds this factorisation inside an invertible triangular transform whose parameters are produced by a masked network [34]. Furthermore, we train a 1-D flow ( $d=1$ ) to approximate the marginal density  $f_{Y_w|\mathcal{H}_1}(y)$ . The autoregressive density estimators [42] in MAF can model each conditional PDF  $f(y_t|y_1, \dots, y_{t-1})$  as a parametric density, whose parameters are produced by hidden layer activations constrained by autoregressive masks, as shown in Fig. 1.

Prior to flow training, we standardise each observation by  $y' = (y - \mu)/\sigma$ , where  $\mu$  and  $\sigma$  are the empirical mean and standard deviation of the  $\mathcal{H}_1$  training set at the same power level. During inference the log-likelihood is corrected by subtracting  $\log \sigma$  to recover the original scale. Specifically, MAF, as a generative density estimation technique from the family of NFs, models a certain probability distribution through an invertible and differentiable mapping between the data space and a simple latent distribution. Mathematically, given an observation set  $\mathcal{Y} = \{y_1, \dots, y_{T_w}\}$  (each observation is the sum of  $N$  power expressed in (8)) with unknown distribution  $f_{Y_w|\mathcal{H}_1}(y)$ , the MAF defines a reversible transformation  $\mathcal{Z} = \mathcal{T}(\mathcal{Y})$  mapping  $\mathcal{Y}$  to a latent variable  $\mathcal{Z}$  with a known simple distribution  $p(z)$ , typically the standard Gaussian, i.e.,  $\mathcal{Z} \sim \mathcal{N}(\mathbf{0}, \mathbf{I}_{T_w})$ . Consequently, the PDF of the observation  $Y_w$  under  $\mathcal{H}_1$  can be expressed via the change of variables formula as

$$f_{Y_w|\mathcal{H}_1}(y) = p(z) \left| \det \left( \frac{\partial z}{\partial y} \right) \right|. \quad (21)$$

As illustrated in Fig. 1, the MAF model is employed to explicitly model  $f_{Y_w|\mathcal{H}_1}(y)$  by leveraging the autoregressive decomposition presented earlier. In MAF, the transformation for each dimension  $y_t$  in (20) is parameterized as

$$z_t = \frac{y_t - \mu_t(y_{<t})}{\sigma_t(y_{<t})}, \quad t = 1, \dots, T_w, \quad (22)$$

where  $\mu_t(y_{<t})$  and  $\sigma_t(y_{<t})$  denote the conditional mean and standard deviation functions that are predicted by a carefully designed masked autoencoder for distribution estimation (MADE) network. The MADE network ensures a strictly autoregressive property through an explicit masking strategy applied to its weight matrices. More specifically, MADE imposes binary masks  $\mathbf{M}_{ij}$  on its fully-connected layers, which are mathematically defined as

$$\mathbf{M}_{ij} = \begin{cases} 1, & \text{if } i \geq j, \\ 0, & \text{otherwise.} \end{cases} \quad (23)$$

where  $i$  is the index of hidden node,  $j$  is the index of input node. The masking structure expressed in (23) strictly enforces each output dimension  $y_t$  to depend only on preceding dimensions  $y_{<t}$ , thus ensuring the autoregressive factorization remains valid. To increase modelling capacity, every second MADE block receives the input in reversed order. It is worth

noting that a deterministic degree assignment can be substituted to guarantee strict monotonicity as in (23). This permutation (implemented as a tensor flip in the forward pass) allows the flow to capture dependencies that a single fixed ordering cannot. Consequently, the Jacobian of the transformation in (21) is a triangular matrix, facilitating efficient computation of the determinant. In practice we accumulate the Jacobian in log-space, i.e.,

$$\log \left( \left| \det \left( \frac{\partial z}{\partial y} \right) \right| \right) = - \sum_{t=1}^{T_w} \sigma_t(y_{<t}). \quad (24)$$

In the training phase, our scheme estimates the parameters  $\theta$  of the MAF model by maximum likelihood estimation (MLE). Given  $T_w$  independent scalar observations  $\{y\}_{i=1}^N$  under the alternative hypothesis  $\mathcal{H}_1$ , the training objective is to maximize the total log-likelihood, i.e.,

$$\theta_{\text{MLE}} = \arg \max_{\theta} \sum_{t=1}^{T_w} \log f_{Y_w|\mathcal{H}_1}(y_t; \theta). \quad (25)$$

Equivalently, we minimize the average negative log-likelihood (NLL) over the  $T_w$  independent scalar observations, defined explicitly as

$$\mathcal{L}(\theta) = - \frac{1}{T_w} \sum_{t=1}^{T_w} \left( \log p(z_t; \theta) + \log \left| \det \left( \frac{\partial z_t}{\partial y_t} \right) \right| \right). \quad (26)$$

In practice, this optimization in (26) is performed using the ADAM algorithm [43]. Within each training iteration,  $z_t = \mathcal{T}(y_t; \theta)$  denotes the autoregressive transformation defined by the MAF.

After estimating the PDF of the observation  $Y_w$  generating from the alternative hypothesis  $\mathcal{H}_1$ , i.e.,  $f_{Y_w|\mathcal{H}_1}(y)$ , the LLR can be calculated as

$$\Lambda(y) = \log \frac{f_{Y_w|\mathcal{H}_1}(y)}{f_{Y_w|\mathcal{H}_0}(y)} = \log \left( \frac{f_{Y_w|\mathcal{H}_0}(y)}{\frac{1}{\Gamma(N)(\delta_w^2)^N} y^{N-1} e^{-\frac{y}{\delta_w^2}}} \right), y \geq 0. \quad (27)$$

Consequently, Willie can perform the optimal detection based on the Neyman-Pearson Lemma. More specifically, for a given FAR  $\alpha$ , the optimal detection threshold  $\eta_o$  can be computed from

$$\mathbb{P}_{\mathcal{H}_0}(\Lambda(y) > \eta_o) = \int_{\Lambda(y) > \eta_o} f_{Y_w|\mathcal{H}_0}(y) dy = \alpha. \quad (28)$$

In practice, the analytical evaluation of the integral in (28) is generally intractable, especially when  $f_{Y_w|\mathcal{H}_1}(y)$  is estimated through MAF. Therefore, in this work, a Monte Carlo simulation approach is employed to empirically determine  $\eta_o$ . Specifically, a large number  $N_m$  of independent samples  $\{y^{(i)}\}_{i=1}^{N_m}$  are generated under the null hypothesis distribution,

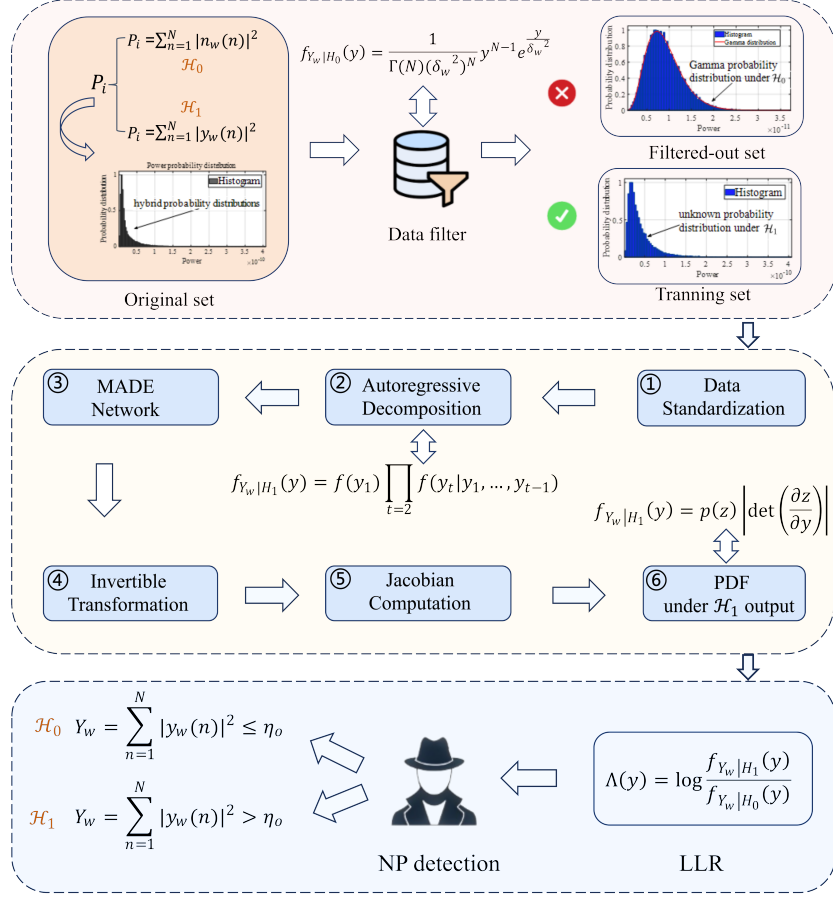


**Figure 2** Schematic diagram of the proposed unsupervised MAF-based Neyman-Pearson detection framework.

i.e., the Gamma distribution in (15). Subsequently, the empirical distribution of the LLR under hypothesis  $\mathcal{H}_0$  is constructed by evaluating each sampled instance, i.e.,

$$\Lambda(y^{(i)}) = \log f_{Y_w|\mathcal{H}_1}(y^{(i)}) - \log f_{Y_w|\mathcal{H}_0}(y^{(i)}). \quad (29)$$

where  $i = 1, 2, \dots, N_m$ . By sorting the obtained LLR values, the optimal detection threshold  $\eta_o$  is empirically estimated as the  $(1 - \alpha)$ -quantile of the LLR distribution under hypothesis  $\mathcal{H}_0$ . Formally, the optimal detection threshold  $\eta_o$  is computed as

$$\eta_o = F_{\Lambda(y)|\mathcal{H}_0}^{-1}(1 - \alpha), \quad (30)$$

where  $F_{\Lambda(y)|\mathcal{H}_0}^{-1}$  denotes the empirical inverse cumulative distribution function obtained from the sampled data  $\{y^{(i)}\}_{i=1}^{N_m}$ .

However, during MAF training, the training set  $\mathcal{Y}$  must be labeled so that the PDF  $f_{Y_w|\mathcal{H}_1}(y)$  under the alternative hypothesis  $\mathcal{H}_1$  can be effectively learned. In practical covert communication scenarios, it is overly idealistic to assume that the warden Willie has access to labeled observations, i.e., that he knows with certainty whether Alice and Bob are transmitting or not. Therefore, a more robust approach is to use unsupervised learning to model the PDF  $f_{Y_w|\mathcal{H}_1}(y)$  for the NP detection.

As expressed in (1), in covert communications, the received signal at Willie constitutes a binary hypothesis testing problem involving two hypotheses, i.e.,  $\mathcal{H}_1$  and  $\mathcal{H}_0$ . Accordingly, the observations at Willie, as presented in (8), correspond solely to these two possible cases. Based on the derivation in (15), we have the prior knowledge that the Willie's observations under  $\mathcal{H}_0$  follow a deterministic Gamma distribution.

Therefore, the original observation set  $\mathcal{Y} = \{y_1, y_2, \dots, y_{T_w}\}$  collected at Willie can be preprocessed by applying a prior Gamma distribution model to filter out observations that exhibit high likelihood under the null hypothesis  $\mathcal{H}_0$ . More specifically, based on the PDF  $f_{Y_w|\mathcal{H}_0}(y)$  given in (15), the likelihood of each observation  $\mathcal{Y}$  under  $\mathcal{H}_0$  can be defined as

$$p_t|_{\mathcal{H}_0} \stackrel{\Delta}{=} f_{Y_w|\mathcal{H}_0}(y_t) = \frac{1}{\Gamma(N) (\delta_w^2)^N} (y_t)^{N-1} e^{-\frac{y_t}{\delta_w^2}}, \quad (31)$$

where  $t = 1, 2, \dots, T_w$ .

Let  $\rho \in (0, 1)$  denote the proportion of observations to be discarded. To remove observations with high likelihood under  $\mathcal{H}_0$ , we define a threshold  $\tau_\rho$  as the smallest value satisfying

the following condition:

$$\tau_\rho = \inf \left\{ i \left| \frac{1}{T_w} \sum_{i=1}^{T_w} \mathbf{1}(p_t|_{\mathcal{H}_0} \geq i) \leq \rho \right. \right\}, \quad (32)$$

where  $\mathbf{1}(\cdot)$  is the indicator function. That is,  $\tau_\rho$  corresponds to the  $(1 - \rho)$  empirical quantile of the likelihood scores in  $\mathcal{Y}$ .

Based on this threshold  $\tau_\rho$ , the observation set  $\mathcal{Y}$  is partitioned as follows:

$$\bar{\mathcal{Y}} = \left\{ y_t \in \mathcal{Y} \mid p_t|_{\mathcal{H}_0} \geq \tau_\rho \right\}, \quad (33)$$

where  $\bar{\mathcal{Y}}$  contains samples highly likely to belong to  $\mathcal{H}_0$ . As a result, the remaining set  $\tilde{\mathcal{Y}} = \mathcal{Y} \setminus \bar{\mathcal{Y}} = \{\tilde{y}_t\}$  is retained for training the PDF of the PDF  $f_{Y_w|\mathcal{H}_1}(y)$  under the alternative hypothesis  $\mathcal{H}_1$ .

The proposed unsupervised MAF-based NP detection framework for the warden Willie to detect covert communications between Alice and Bob is schematically illustrated in Fig. 2.

### 3.3 Impact of DRIS on Covert Communications Between Alice and Bob

According to the SJNR defined in (11), it can be seen that the implementation of the DRIS also affects the communication performance between Alice and Bob. In order to quantify the impact of DRIS on the covert communications between Alice and Bob, we first derive the following statistical characteristic of the DRIS-jammed channel  $h_D^b(t)$  in Proposition 2.

**Proposition 2** The random and time-varying DRIS-based term  $h_D^b(t)$  converges in distribution to a complex Gaussian discussion as  $N_D \rightarrow \infty$ , i.e.,

$$h_D^b(t) = \frac{\widehat{g} \text{diag}(\varphi(t)) \widehat{h}_1^b}{\mathcal{L}^{\frac{v_g}{2}} \mathcal{L}^{\frac{v_I^b}{2}}} \xrightarrow{d} \mathcal{CN} \left( 0, \frac{N_D \bar{\alpha}}{\mathcal{L}^{v_g} L^{v_I^b}} \right). \quad (34)$$

**Proof** See Appendix 5.2.

Conditioned on the fact that the covert symbol  $s(m)$  is independent of the wireless channels, the SJNR in (11) can be reduced to

$$\gamma_b = \frac{\mathbb{E}[|h_d^b|^2] \mathbb{E}[|s(m)|^2]}{\mathbb{E}[|h_D^b(m)s(m)|^2] + \delta_b^2}. \quad (35)$$

Substituting (34) into (35), we have

$$\gamma_b \xrightarrow{d} \frac{\frac{P_0}{\mathcal{L}^{v_I^b}}}{\frac{P_0 N_D \bar{\alpha}}{\mathcal{L}^{v_g} \mathcal{L}^{v_I^b}} + \delta_b^2}, \text{ as } N_D \rightarrow \infty. \quad (36)$$

In traditional covert communications, while higher transmit power improves the communication performance between Alice and Bob, it also increases the probability of detection by

the warden Willie. However, in the cover communication system in the presence of a DRIS, it can be seen from (36) that increasing transmit power  $P_0$  not only results in a higher detection probability at the warden, but also amplifies the DRIS-induced jamming term, i.e.,  $\frac{P_0 N_D \bar{\alpha}}{\mathcal{L}^{v_g} \mathcal{L}^{v_I^b}}$ , which degrades the communication performance between Alice and Bob rather than enhancing it. The DRIS not only jams the covert transmissions between Alice and Bob, but also decreases the error probabilities of Willie's detections, even without either Bob's channel knowledge or additional jamming power.

## 4 Simulation Results and Discussion

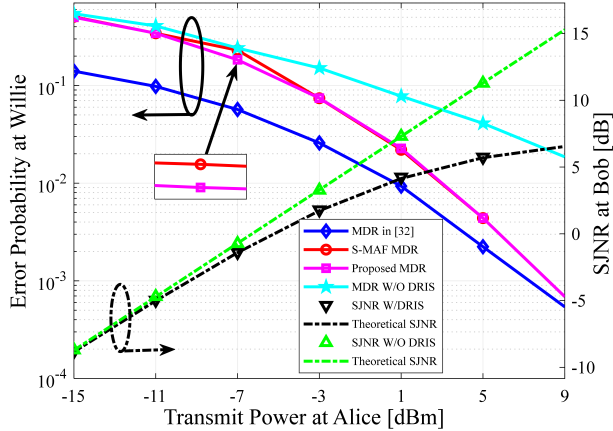
In this section, we perform Monte Carlo simulations to evaluate the impact of the DRIS on covert communications and to validate our theoretical analysis and the proposed unsupervised MAF-based NP detector in Section 3. Unless otherwise stated, the default parameters are as follows. Alice, equipped with a single antenna, is located at (0 m, 0 m, 5 m), while Bob, also equipped with a single antenna, is uniformly distributed within an annular region centered at (0 m, 140 m, 0 m) with inner and outer radii of 10 m and 20 m, respectively. The warden Willie is positioned at (0 m, 100 m, 0 m) to monitor potential covert transmissions. A DRIS consisting of 2048 reflective elements ( $N_{D,h} = 64, N_{D,v} = 32$ ) is deployed at  $(-d_{AD} \text{ m}, 0 \text{ m}, 5 \text{ m})$ , with the distance between Alice and the DRIS center set to  $d_{AD} = 1.5 \text{ m}$ . The DRIS employs 1-bit quantized reflection coefficients, with phase shifts chosen equiprobably from  $\Psi = \{\frac{\pi}{9}, \frac{7\pi}{6}\}$  and their corresponding amplitudes determined by the hardware mapping  $\Omega = \mathcal{F}(\Theta) = \{0.8, 1\}$  [16]. This configuration results in  $\bar{\alpha} = 0.82$ , consistent with Proposition 1.

The received signals at Willie are processed using the detection rule in (8), accumulating  $N = 5$  samples within each channel coherence interval. Large-scale fading parameters follow 3GPP standards [44] as specified in Table 1. The AWGN variance is  $\sigma_c^2 = -170 + 10\log_{10}(BW) \text{ dBm}$  with  $BW = 180 \text{ kHz}$ . We implement an MAF model trained in an unsupervised manner on prefiltered received power statistics for the AI-based detection. The model architecture incorporates 5 autoregressive layers with 64 hidden units each, optimized using Adam with a learning rate of  $2 \times 10^{-4}$  over 200 epochs.

Fig. 3 illustrates Willie's MDR on the left y-axis and Bob's SJNR (dB) on the right y-axis versus Alice's transmit power. The legend comprises: (i) the MDR of the baseline method in [32] (MDR in [32]); (ii) the MDR of the supervised MAF-based NP detector (S-MAF MDR); and (iii) the MDR of the proposed method (Proposed MDR). (iv) MDR without DRIS (MDR W/O DRIS); (v) simulated/theoretical SJNR with DRIS (SJNR W/ DRIS; theoretical SJNR); and (vi) simu-

**Table 1** Wireless Channel Simulation Parameters

Large-scale Parameter	Value
LoS fading	$35.6 + 22\log_{10}(d)$ (dB)
NLoS fading	$32.6 + 36.7\log_{10}(d)$

**Figure 3** Relationship between MDR and transmit power (left y-axis), and that between SJNR and transmit power (right y-axis).

lated/theoretical SJNR without DRIS (SJNR W/O DRIS; theoretical SJNR).

The results in Fig. 3 demonstrate that, for a given FAR, introducing DRIS significantly reduces Willie’s MDR while simultaneously jamming Bob’s SJNR, with the SJNR theoretical predictions showing close alignment with the Monte Carlo simulation results. As Alice’s transmit power increases, the MDR monotonically decreases, whereas the SJNR exhibits only marginal improvement. This indicates that simply increasing the power level yields limited channel gain for covert communication, while significantly elevating the risk of detection by Willie. Notably, the proposed unsupervised MAF-based NP detection framework achieves detection performance comparable to that based on the supervised MAF, without requiring labeled data under the  $\mathcal{H}_1$  hypothesis. This demonstrates the proposed method’s ability to effectively learn the underlying  $\mathcal{H}_1$  distribution directly from mixed observations, eliminating the reliance on typically unavailable labeled datasets in practical covert communication scenarios. Although the detection method in [32] attains lower MDR values by leveraging stronger prior information, our proposed unsupervised MAF-based NP detection framework remains highly robust even in the absence of CSI.

Fig. 4 compares Willie’s MDR (left y-axis) with Bob’s SJNR (right y-axis) as functions of the number of DRIS elements for various baseline schemes. Results are presented for both low (-7 dBm) and high (5 dBm) transmit power at Alice. As shown in Fig. 4, increasing the number of DRIS elements reduces the MDR for a given FAR. Moreover, this reduction in MDR is accelerated by higher transmit power from Alice.

This is clearly evidenced in Fig. 4 (a) and (b), which show that Willie’s detection error probabilities diminish more rapidly at higher transmit power. In addition, Fig. 4 (a) and (b) reveal that Bob’s SJNR decreases with an increasing number of DRIS elements, implying that Willie can leverage more DRIS elements not only to enhance his detection accuracy but also to disrupt the covert communication between Alice and Bob more effectively. Furthermore, in agreement with Propositions 1 and 2, the SJNR of the DRIS-induced ACA at Bob’s location approaches zero as the number of DRIS elements tends to infinity. The close agreement between simulation results and theoretical analysis validates the mathematical derivations presented in Propositions 1 and 2.

Fig. 5 presents the MDR and the SJNR versus the number of Willie’s detection samples  $N$  under a given FAR. According to (8), the test statistic  $Y_w = \sum_{n=1}^N |y_w(n)|^2$  accumulates  $N$  detection samples. Under  $\mathcal{H}_0$ ,  $Y_w$  follows a Gamma distribution with shape parameter  $N$ . As  $N$  increases, the test statistic  $Y_w$  becomes more concentrated, improving the separability between  $\mathcal{H}_0$  and  $\mathcal{H}_1$  and yielding a monotonic reduction in MDR. As illustrated in Fig. 5 (a), the decline is modest at low transmit power due to the weak covert signal and the gradual accrual of averaging gains. However, it becomes steep at high transmit power, as shown in Fig. 5 (b). This indicates that higher transmit power, together with more detection samples, markedly enhance the Willie’s detection accuracy. In contrast, the SJNR at Bob is essentially independent of  $N$  and aligns with the theoretical curve because it is influenced by the Alice-Bob channel and DRIS-induced jamming rather than Willie’s sampling strategy. Specifically, the choice of  $N$  is constrained by the length of a channel coherence interval, i.e.,  $N \leq M$ , where  $M$  denotes the maximum number of detection samples that can be acquired within a channel coherence interval. The above results indicate that, within a single channel coherence interval, increasing the number of detection samples is an effective means for Willie to reduce detection error probabilities.

## 5 Conclusions

In this paper, we investigated covert communications in the presence of a DRIS and proposed a novel unsupervised MAF-based NP detection framework. The proposed detection framework enables the warden Willie to effectively detect covert communications between Alice and Bob even in the absence of CSI. The introduction of DRIS simultaneously reduces Willie’s detection error probabilities and degrades the communication performance between Alice and Bob, without requiring either CSI or additional jamming power. Furthermore, the proposed unsupervised MAF-based NP detection framework does not require labeled datasets, rendering

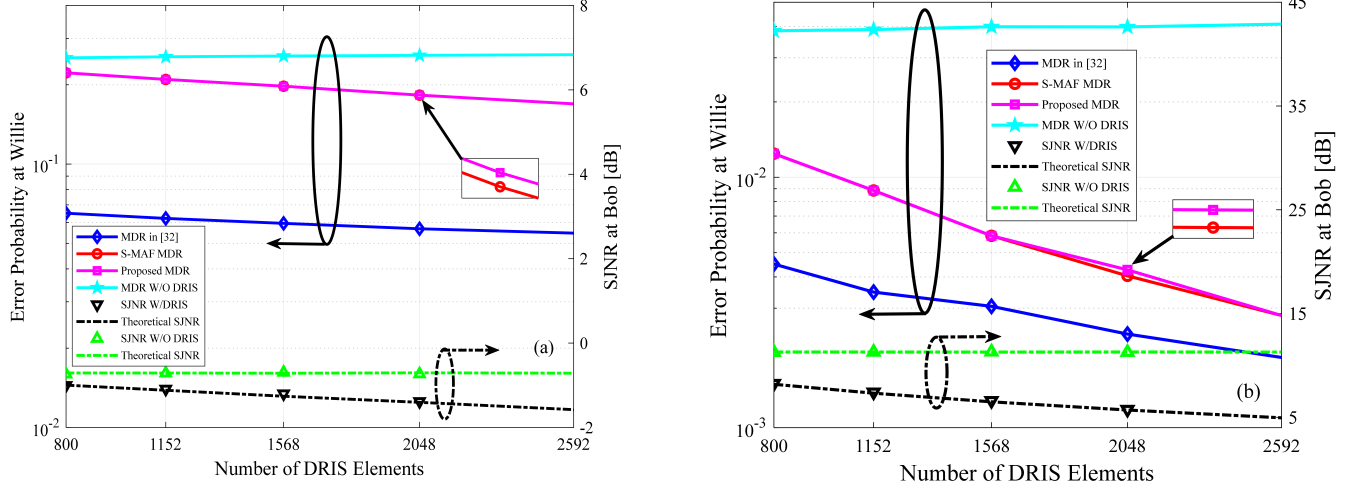


**Figure 4** MDR vs. the number of DRIS elements (left y-axis), and SJNR vs. the number of DRIS elements (right y-axis) at (a) low transmit power (-7 dBm) and (b) high transmit power (5 dBm).

it highly practical and robust in adversarial scenarios. The following conclusions can be drawn from the integration of theoretical modelling and numerical results.

1) The proposed MAF-based NP detection framework operates in an unsupervised manner by leveraging the prior knowledge that the Willie's test statistic under  $\mathcal{H}_0$  follows a specific Gamma distribution. Based on this prior knowledge, the MAF model can be used to filter out high-likelihood  $\mathcal{H}_0$  data. This enables the MAF model to learn the complex distribution of the test statistic under  $\mathcal{H}_1$ , providing a near-optimal approach to implementing the NP detection without ground-truth labels. Simulation results show that the proposed unsupervised MAF-based NP detector achieves a performance level comparable to that of the supervised method. This indicates that it can accurately learn the  $\mathcal{H}_1$  distribution directly from mixed observations without the need for labelled data.

2) The DRIS with random and time-varying reflection coefficients disrupts the channel reciprocity in conventional TDD systems by introducing ACA. The introduction of DRIS not only jams the covert communications between Alice and Bob but also reduces Willie's decision error probabilities, without relying on either CSI or additional jamming power. Moreover, to effectively monitor the covert communications between Alice and Bob, and to maximise the effectiveness of the DRIS-induced ACA, it is preferable for the warden Willie to deploy the DRIS in close proximity to Alice.

3) Due to the DRIS-induced ACA, increasing Alice's transmit power does not notably enhance communication performance. However, higher transmit power leads to higher detection accuracy at Willie while also intensifying the DRIS-induced ACA on the Alice-Bob transmission. It is worth noting that a DRIS with only 1-bit quantization phase shifts is

enough to simultaneously expose and jam covert communications.

Our work demonstrates an effective unsupervised MAF-based NP detection framework for covert communications in the presence of a DRIS, without requiring labeled datasets or additional jamming power. Therefore, it is essential for Alice to investigate some potential countermeasures, such as signal classification, anomaly detection techniques, and adaptive beamforming.

## Appendix

### 5.1 Proof of Proposition 1

Based on the cascaded DRIS-based channel between Alice and Willie expressed in (2) and the definition that  $\varphi(t) = [\beta_1(t)e^{j\varphi_1(t)}, \dots, \beta_{N_D}(t)e^{j\varphi_{N_D}(t)}]$ , we can rewrite  $h_D^W(t)$  as

$$h_D^W(t) = \sqrt{\frac{\varepsilon_g}{(\varepsilon_g + 1)\mathcal{L}^{v_g}\mathcal{L}^{v_I^W}}} \sum_{r=1}^{N_D} [\hat{g}^{\text{LOS}}]_r [\hat{h}_I^W]_r \beta_r(t) e^{j\varphi_r(t)} \\ + \sqrt{\frac{1}{(\varepsilon_g + 1)\mathcal{L}^{v_g}\mathcal{L}^{v_I^W}}} \sum_{r=1}^{N_D} [\hat{g}^{\text{NLOS}}]_r [\hat{h}_I^W]_r \beta_r(t) e^{j\varphi_r(t)}. \quad (37)$$

Assuming that  $\hat{h}_I^W$ ,  $\varphi(t)$ , and  $\hat{g}$  consist of independent i.i.d. elements and  $\mathbb{E}[\hat{h}_I^W] = 0$ , the expectations of the terms in (37) are obtained as follows:

$$\mathbb{E}[[\hat{g}^{\text{LOS}}]_r [\hat{h}_I^W]_r \beta_r(t) e^{j\varphi_r(t)}] \\ = \mathbb{E}[\hat{g}^{\text{LOS}} \beta_r(t) e^{j\varphi_r(t)}]_r \mathbb{E}[\hat{h}_I^W]_r = 0, \quad (38)$$

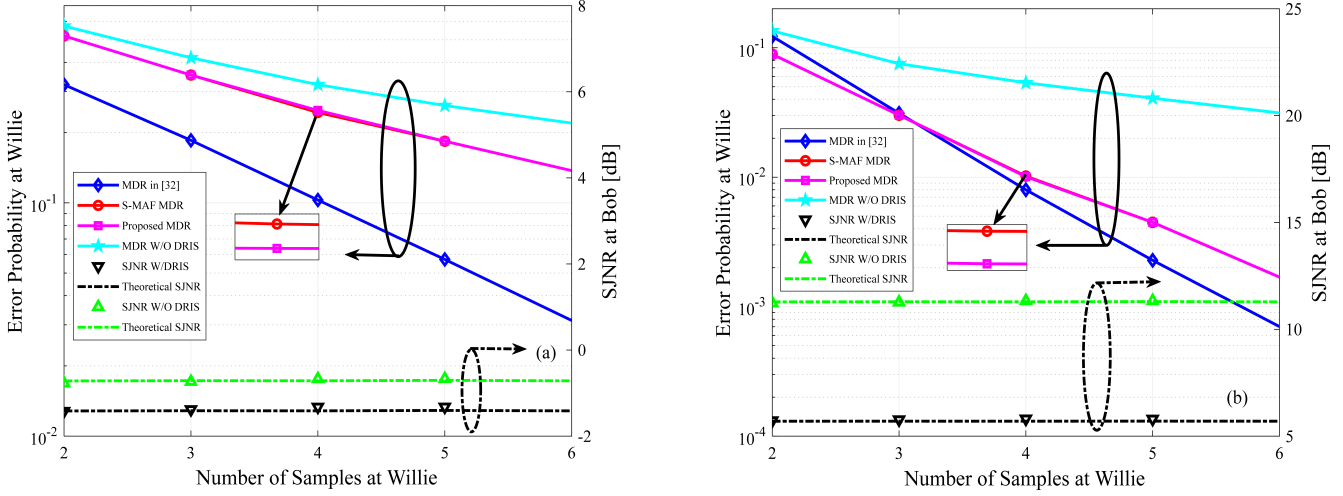


**Figure 5** MDR vs. the number of Willie's detections (left y-axis), and SJNR vs. the number of Willie's detections (right y-axis) at (a) low transmit power (-7 dBm) and (b) high transmit power (5 dBm).

$$\begin{aligned} & \mathbb{E} \left[ [\hat{\mathbf{g}}^{\text{NLOS}}]_r [\hat{\mathbf{h}}_I^W]_r \beta_r(t) e^{j\varphi_r(t)} \right] \\ &= \mathbb{E} [\hat{\mathbf{g}}^{\text{NLOS}} \beta_r(t) e^{j\varphi_r(t)}]_r \mathbb{E} [\hat{\mathbf{h}}_I^W]_r = 0. \end{aligned} \quad (39)$$

Furthermore, the corresponding variances are expressed as

$$\text{Var} \left[ [\hat{\mathbf{g}}^{\text{LOS}}]_r [\hat{\mathbf{h}}_I^W]_r \beta_r(t) e^{j\varphi_r(t)} \right] = \mathbb{E} \left[ |[\hat{\mathbf{h}}_I^W]_r|^2 \right] \mathbb{E} \left[ |\beta_r(t)|^2 \right], \quad (40)$$

where

$$\mathbb{E} \left[ |\beta_r(t)|^2 \right] = \sum_{i=1}^b P_i \alpha_i^2 = \bar{\alpha}, \quad (41)$$

$P_i$  denotes the probability that the DRIS phase shift  $\varphi_r(t)$  takes the  $i$ -th value  $\phi_i \in \Omega$ , i.e.,  $P_i = \mathbb{P}(\varphi_r(t) = \phi_i), \forall r$ .

Consequently, the variances in (40) can be obtained as

$$\text{Var} \left[ [\hat{\mathbf{g}}^{\text{LOS}}]_r [\hat{\mathbf{h}}_I^W]_r \beta_r(t) e^{j\varphi_r(t)} \right] = \bar{\alpha}, \quad (42)$$

Take the same steps as above, we can obtain that

$$\begin{aligned} & \text{Var} \left[ [\hat{\mathbf{g}}^{\text{NLOS}}]_r [\hat{\mathbf{h}}_I^W]_r \beta_r(t) e^{j\varphi_r(t)} \right] \\ &= \mathbb{E} \left[ |[\hat{\mathbf{g}}^{\text{NLOS}}]_r|^2 \right] \mathbb{E} \left[ |[\hat{\mathbf{h}}_I^W]_r|^2 \right] \mathbb{E} \left[ |\beta_r(t)|^2 \right] = \bar{\alpha}. \end{aligned} \quad (43)$$

When  $N_D$  is sufficiently large, according to the Lindeberg–Lévy central limit theorem, the normalized sum converges in distribution to a circularly-symmetric complex Gaussian random variable, i.e.,

$$h_D^W(t) = \frac{\hat{\mathbf{g}} \text{diag}(\varphi(t)) \hat{\mathbf{h}}_I^W}{\mathcal{L}^{\frac{v_g}{2}} \mathcal{L}^{\frac{v_I^W}{2}}} \xrightarrow{d} \mathcal{CN} \left( 0, \frac{N_D \bar{\alpha}}{\mathcal{L}^{\frac{v_g}{2}} \mathcal{L}^{\frac{v_I^W}{2}}} \right). \quad (44)$$

## 5.2 Proof of Proposition 2

The proof is analogous to that in Appendix 5.1.

## References

- [1] A. Mukherjee, S. A. A. Fakoorian, J. Huang, and A. L. Swindlehurst, “Principles of physical layer security in multiuser wireless networks: A survey,” *IEEE Commun. Surv. Tut.*, vol. 16, no. 3, pp. 1550–1573, Third Quarter 2014.
- [2] X. Chen, J. An, Z. Xiong, C. Xing, N. Zhao, F. R. Yu, and A. Nallanathan, “Covert communications: A comprehensive survey,” *IEEE Commun. Surv. Tut.*, vol. 25, no. 2, pp. 1173–1198, 2nd Quarter 2023.
- [3] T. V. Sobers, B. A. Bash, S. Guha, D. Towsley, and D. Goeckel, “Covert communication in the presence of an uninformed jammer,” *IEEE Trans. Wireless Commun.*, vol. 16, no. 9, pp. 6193–6206, Sept. 2017.
- [4] K. Li, P. A. Kelly, and D. Goeckel, “Optimal power adaptation in covert communication with an uninformed jammer,” *IEEE Trans. Wireless Commun.*, vol. 19, no. 5, pp. 3463–3473, May 2020.
- [5] Abdelaziz A, Koksal C E. Fundamental limits of covert communication over MIMO AWGN channel. In: IEEE Conference on Communications and Network Security, 2013, 31: 1921–1930
- [6] B. A. Bash, D. Goeckel, and D. Towsley, “Limits of reliable communication with low probability of detection on AWGN channels,” *IEEE J. Sel. Areas Commun.*, vol. 31, no. 9, pp. 1921–1930, Sept. 2013.
- [7] X. Chen, W. Sun, C. Xing, N. Zhao, Y. Chen, F. R. Yu, and A. Nallanathan, “Multi-antenna covert communica-

tion via full-duplex jamming against a warden with uncertain locations,” *IEEE Trans. Wireless Commun.*, vol. 20, no. 8, pp. 5467–5480, Aug. 2021.

[8] T.-X. Zheng, Z. Yang, C. Wang, Z. Li, J. Yuan, and X. Guan, “Wireless covert communications aided by distributed cooperative jamming over slow fading channels,” *IEEE Trans. Wireless Commun.*, vol. 20, no. 11, pp. 7026–7039, Nov. 2021.

[9] S. A. Ahmadzadeh and G. B. Agnew, “Turbo covert channel: An iterative framework for covert communication over data networks,” in *Proc. IEEE INFOCOM*, Turin, Italy, Jul. 2013, pp. 2031–2039.

[10] L. Tao, W. Yang, S. Yan, D. Wu, X. Guan, and D. Chen, “Covert communication in downlink NOMA systems with random transmit power,” *IEEE Wireless Commun. Lett.*, vol. 9, no. 11, pp. 2000–2004, Nov. 2020.

[11] O. A. Topal and G. Karabulut-Kurt, “Covert communication in cooperative NOMA networks,” in *Proc. IEEE SIU*, Gaziantep, Turkey, Oct. 2020.

[12] J. Hu, S. Yan, X. Zhou, F. Shu, J. Li, and J. Wang, “Covert communication achieved by a greedy relay in wireless networks,” *IEEE Trans. Wireless Commun.*, vol. 17, no. 7, pp. 4766–4779, Jul. 2018.

[13] M. Lin, C. Liu, and W. Wang, “Relay-assisted uplink covert communication in the presence of multi-antenna warden and uninformed jamming,” *IEEE Trans. Commun.*, vol. 72, no. 4, pp. 2124–2137, Apr. 2024.

[14] R. Sun, B. Yang, S. Ma, Y. Shen, and X. Jiang, “Covert rate maximization in wireless full-duplex relaying systems with power control,” *IEEE Trans. Commun.*, vol. 69, no. 9, pp. 6198–6212, Sep. 2021.

[15] J. Hu, K. Shahzad, S. Yan, X. Zhou, F. Shu, and J. Li, “Covert communications with a full-duplex receiver over wireless fading channels,” in *Proc. IEEE Int. Commun. Conf. (ICC’18)*, Kansas City, MO, May 2018.

[16] H. Zhang, S. Zeng, B. Di, Y. Tan, M. D. Renzo, M. Debbah, Z. Han, H. V. Poor, and L. Song, “Intelligent omni-surfaces for full-dimensional wireless communications: Principles, technology, and implementation,” *IEEE Commun. Mag.*, vol. 60, no. 2, pp. 39–45, Feb. 2022.

[17] C. Huang, S. Hu, G. C. Alexandropoulos, A. Zappone, C. Yuen, R. Zhang, M. Di Renzo, and M. Debbah, “Holographic MIMO surfaces for 6G wireless networks: Opportunities, challenges, and trends,” *IEEE Wireless Commun.*, vol. 27, no. 5, pp. 118–125, Jul. 2020.

[18] Q. Wu and R. Zhang, “Intelligent reflecting surface enhanced wireless network via joint active and passive beamforming,” *IEEE Trans. Wireless Commun.*, vol. 18, no. 11, pp. 5394–5409, Nov. 2019.

[19] Q. Wu, S. Zhang, B. Zheng, C. You, and R. Zhang, “Intelligent reflecting surface aided wireless communications: A tutorial,” *IEEE Trans. Commun.*, vol. 69, no. 5, pp. 3313–3351, Jan. 2021.

[20] S. Gong, X. Lu, D. T. Hoang, D. Niyato, L. Shu, D. I. Kim, and Y.-C. Liang, “Toward smart wireless communications via intelligent reflecting surfaces: A contemporary survey,” *IEEE Commun. Surv. Tut.*, vol. 22, no. 4, pp. 2283–2314, Fourth Quarter 2020.

[21] R. Deng, B. Di, H. Zhang, Y. Tan, and L. Song, “Reconfigurable holographic surface-enabled multi-user wireless communications: Amplitude-controlled holographic beamforming,” *IEEE Trans. Wireless Commun.*, vol. 21, no. 8, pp. 6003–6017, Aug. 2022.

[22] T. Cui, M. Qi, X. Wan, J. Zhao, and Q. Cheng, “Coding metamaterials, digital metamaterials and programmable metamaterials,” *Light-Sci. Appl.*, vol. 3, p. e218, Oct. 2014.

[23] C. Huang, A. Zappone, G. C. Alexandropoulos, M. Debbah, and C. Yuen, “Reconfigurable intelligent surfaces for energy efficiency in wireless communication,” *IEEE Trans. Wireless Commun.*, vol. 18, no. 8, pp. 4157–4170, Jun. 2019.

[24] C. Huang, R. Mo, and C. Yuen, “Reconfigurable intelligent surface assisted multiuser MISO systems exploiting deep reinforcement learning,” *IEEE J. Sel. Areas Commun.*, vol. 38, no. 8, pp. 1839–1850, Aug. 2020.

[25] L. Lv, Q. Wu, Z. Li, Z. Ding, N. Al-Dhahir, and J. Chen, “Covert communication in intelligent reflecting surface-assisted NOMA systems: Design, analysis, and optimization,” *IEEE Trans. Wireless Commun.*, vol. 21, no. 3, pp. 1735–1750, Mar. 2022.

[26] C. Wang, Z. Xiong, M. Zheng, N. Zhao, and D. Niyato, “Covert communications via two-way IRS with noise power uncertainty,” *IEEE Trans. Commun.*, vol. 72, no. 8, pp. 4803–4815, Aug. 2024.

[27] Y. Wu, X. Chen, M. Liu, L. Xu, N. Zhao, X. Wang, and D. W. K. Ng, “IRS-assisted covert communication with equal and unequal transmit prior probabilities,” *IEEE Trans. Commun.*, vol. 72, no. 5, pp. 2897–2912, May 2024.

[28] C. Wang, X. Chen, J. An, Z. Xiong, C. Xing, N. Zhao, and D. Niyato, “Covert communication assisted by UAV-IRS,” *IEEE Trans. Commun.*, vol. 71, no. 1, pp. 357–369, Jan. 2023.

[29] Q. Wang, S. Guo, C. Wu, C. Xing, N. Zhao, D. Niyato, and G. K. Karagiannidis, “STAR-RIS aided covert communication in UAV air-ground networks,” *IEEE J. Sel. Areas Commun.*, vol. 43, no. 1, pp. 245–258, Jan. 2025.

[30] H. Huang, L. Dai, H. Zhang, C. Zhang, Z. Tian, Y. Cai, A. L. Swindlehurst, and Z. Han, “DISCO might not be funky: Random intelligent reflective surface configurations that attack,” *IEEE Wireless Commun.*, vol. 31, no. 5, pp. 76–82, Oct. 2024.

[31] H. Wang, Z. Han and A. L. Swindlehurst, “Channel reciprocity attacks using intelligent surfaces with non-diagonal phase shifts,” *IEEE Open J. Commun. Soc.*, vol. 5, pp. 1469–1485, Feb. 2024.

[32] H. Huang, H. Zhang, Y. Cai, D. Niyato, A. L. Swindlehurst, and Z. Han, “Simultaneously exposing and jamming covert communications via Disco reconfigurable intelligent surfaces,” *arXiv preprint*, arXiv:2505.12213, May 2025. [Online].

[33] I. Kobyzhev, S. J. Prince, and M. A. Brubaker, “Normalizing flows: An introduction and review of current methods,” *IEEE Trans. Pattern Anal. Mach. Intell.*, vol. 43, no. 11, pp. 3964–3979, Nov. 2021.

[34] Papamakarios G, Pavlakou T, and Murray I. Masked autoregressive flow for density estimation. In: Conference on Neural Information Processing Systems, 2017: 1–10

[35] Kingma D P, Salimans T, Jozefowicz R, et al. Improved variational inference with inverse autoregressive flow. In: Conference on Neural Information Processing Systems, 2016: 4743–4751

[36] Kingma D P and Dhariwal P. Glow: Generative flow with invertible 1x1 convolutions. In: Conference on Neural Information Processing Systems, 2018: 10215–10224

[37] Huang H, Zhang Y, Zhang H, Cai Y, Swindlehurst A L, and Han Z. Disco intelligent reflecting surfaces: Active channel aging for fully-passive jamming attacks. *IEEE Transactions on Wireless Communications*, 2024, 23: 806–819

[38] Huang H, Dai L, Zhang H, et al. Anti-jamming pre-coding against disco intelligent reflecting surfaces based fully-passive jamming attacks. *IEEE Transactions on Wireless Communications*, 2024, 23: 9315–9329

[39] Chen Y and Dai L. Non-stationary channel estimation for extremely large-scale MIMO. *IEEE Transactions on Wireless Communications*, 2024, 23: 7683–7697

[40] Cui M and Dai L. Channel estimation for extremely large-scale MIMO: Far-field or near-field? *IEEE Transactions on Communications*, 2022, 70: 2663–2677

[41] O’Donoughue N and Moura J M F. On the product of independent complex Gaussians. *IEEE Transactions on Signal Processing*, 2012, 60: 1050–1063

[42] Uria B, Côté M-A, Gregor K, Murray I, and Larochelle H. Neural autoregressive distribution estimation. *Journal of Machine Learning Research*, 2016, 17: 1–37

[43] Kingma D P and Ba J L. Adam: A method for stochastic optimization. In: International Conference on Learning Representations, 2015: 1–15

[44] Further Advancements for E-UTRA Physical Layer Aspects (Release 9), document 3GPP TS 36.814, Mar. 2010.